

# Al-WC composite coating on AZ91D Mg alloy by low power pulsed laser cladding

Y. Q. Zhang\*, Z. Y. Li, S. Y. Liu, S. Z. Wei

*The Welding Research Center, College of Material Science and Engineering, North University of China, Tai Yuan 030051, P. R. China*

Received 11 February 2019, received in revised form 11 February 2020, accepted 13 February 2020

## Abstract

Laser cladding coatings were fabricated on AZ91D magnesium alloy using Al and WC powders with a weight percentage ratio of 95:5, 90:10, and 85:15 by a low power pulsed Nd:YAG laser. During the process of laser cladding, most of WC was decomposed. Tiny white granular resultant  $\text{Al}_{18}\text{Mg}_3\text{W}_2$  was detected in all coatings, while bright white  $\text{Al}_4\text{W}$  particles with clustering tendency were found only in the 10 and 15 wt.% WC coatings because of relatively high WC content.  $\alpha$ -Al,  $\alpha$ -Mg,  $\text{Al}_3\text{Mg}_2$ , and  $\text{Al}_{12}\text{Mg}_{17}$  were also detected at the coatings. The hardness of the coatings increased by 3–4 times compared with that of the substrate. The corrosion resistance of the coatings was also improved markedly, mainly the passivation phenomenon was observed in all coatings, which may benefit from the formation of oxidation film  $\text{Al}_2\text{O}_3 \cdot \text{H}_2\text{O}$  on the surface of the coatings due to high Al concentration.

**Key words:** laser cladding, magnesium alloy, corrosion, WC, Al

## 1. Introduction

Magnesium and magnesium alloy have been used widely in automobile, electronics, aerospace, and national defense industries as high performance lightweight structural materials by virtue of their merits such as high specific strength and specific stiffness, high damping capacity and excellent machinability [1, 2]. However, nonnegligible disadvantages, including poor corrosion and wear resistance, impede the further application of Mg alloy. It can be improved by surface treatment technologies, including plasma spraying, electroplating, conversion coating, anodic oxidation, vapor deposition and laser treatment [3–6], among which laser cladding has considerable superiority: laser beam with high energy density allows fast heating rate and small heat-affected zone, the control to laser energy may limit dilution ratio (2–8% or less) and reduce the effect of substrate elements on the coating, the fusion of substrate can make sure firm metallurgical bonding between coating and substrate, which make it an excellent method in improving surface performance of magnesium and magnesium alloy.

The cladding powders applied on Mg substrate generally are classified as five types: binary metal powders such as Al-Cu [7], Al-Si [8–10], and Al-Sn [11]; ternary metal powders like Ni-Cu-Al [12], Ni-Zr-Al [13], and Ti-Ni-Al [14]; single pure ceramic powders like SiC [15],  $\text{Al}_2\text{O}_3$  [16] which are in general processed by plasma-spraying followed by laser cladding; mixture powders used to in-situ synthesize ceramic reinforced particle such as Al-Zr- $\text{B}_4\text{C}$  [17], Al-Ti- $\text{B}_4\text{C}$  [18]; mixture powders of metal and ceramic particle like Al- $\text{Al}_2\text{O}_3$  [19], Al-SiC [20, 21], and Al- $\text{Al}_2\text{O}_3$  [22]. Composite coatings in which ceramic particles with a certain size are added directly may improve hardness and wear resistance and corrosion resistance of the coating. For example, Hazra et al. [19] carried out laser cladding coating on MRI 153M Mg alloy using Al- $\text{Al}_2\text{O}_3$  powders.  $\text{Al}_2\text{O}_3$  particles partially or entirely melted during laser irradiation, wear resistance obtained an order of magnitude improvement relative to the substrate. Zheng et al. [20] fabricated the composite coatings with Al-SiC powders on AZ91D Mg alloy by laser cladding. The coatings were composed of SiC and  $\text{Al}_{12}\text{Mg}_{17}$ , whose hardness was improved remarkably.

\*Corresponding author: tel.: +86 13546342801; e-mail address: [yingqiaozhang@nuc.edu.cn](mailto:yingqiaozhang@nuc.edu.cn)

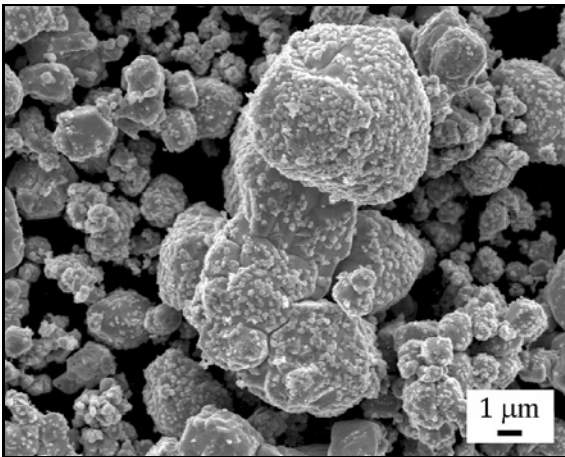


Fig. 1. The macrographs of WC powder.

Table 1. Chemical composition of specimens (wt.%)

Al	Zn	Mn	Si	Be	others	Mg
8.99	0.71	0.25	0.048	0.0071	≤ 0.002	Bal.

Besides  $\text{Al}_2\text{O}_3$ ,  $\text{SiC}$ ,  $\text{TiC}$ , and  $\text{ZrC}$  ceramic powders, which can be added directly into the coating, tungsten carbide is also considered to be one of the most commonly used ceramic powders due to its ultra-high hardness and low thermal expansion coefficient [23]. Fernández et al. [24] added WC as reinforced particles into the laser cladding NiCrBSi coatings on AISI 1045 steel substrate. Hong et al. [25] achieved a nano-structured WC-10Co-4Cr coating by high-velocity oxygen fuel (HVOF) sprayed on Cr12MoV steel. Yet there is almost no research on the laser cladding WC-containing coating on Mg alloys substrate.

In this study, the composite coatings were fabricated on AZ91D Mg alloy using Al-WC powders by a 0.4 kW pulsed low power Nd:YAG laser, which is more favorable in controlling energy input and reducing dilution ratio than high power laser. It was investigated whether or not WC was decomposed during the laser processing and what decomposition and synthetic products were. The properties of coatings were also examined.

## 2. Experimental procedure

### 2.1. Specimen preparation and laser cladding

The AZ91D magnesium alloy plate with dimensions of  $20 \times 15 \times 4 \text{ mm}^3$  was used as the substrate, the chemical composition of which is shown in Table 1. After sanded with 600# SiC sandpaper, the

Table 2. Laser cladding parameters

Processing parameter	Value
Electric current (A)	120
Scanning velocity ( $\text{mm min}^{-1}$ )	150
Frequency (Hz)	20
Pulse width (ms)	4
Beam spot diameter (mm)	0.8
Overlap rate (%)	60
Gas flow ( $\text{L min}^{-1}$ )	9
Average power (W)	400

specimens were cleaned with alcohol and dried in air. Commercial powders of Al (99.9 % purity, 300 mesh) and WC (99.9 % purity, 500 mesh) with weight percentage ratio of 95:5, 90:10, and 85:15 were mixed by ball mill. The morphology of WC powder is shown in Fig. 1. These mixing powders were blended with the binder of 50 vol.% sodium silicate and 50 vol.% water and deposited on the substrate with an average thickness of 400  $\mu\text{m}$ . Laser treatments were carried out on the surface of the specimens using a low power pulsed Nd:YAG laser (1.06  $\mu\text{m}$  wavelength) after drying at room temperature for 24 h. Argon (99.9 % purity) was used as a shielding gas to prevent the coating with high temperature from exposure to the air. The parameters used during laser cladding are shown in Table 2. The experiments proved that the overlap rate had a significant effect on the surface forming of the coating besides laser beam spot diameter and other parameters. Severe spheroidization of coating surface or incomplete melting of cladding powders would happen when the overlap rate was too low; excessive evaporation of low melting point component in the coating or the substrate would occur when overlap rate was too large. A 60 % overlap rate was proved to be suitable in this experiment.

### 2.2. Microstructural examination

Optical microscope (LEICA DM2500M, Germany) and scanning electron microscope SEM (SU5000, Japan) with energy dispersive spectroscopy EDS were used to observe the cross-sectional microstructure and analyze the chemical composition of the coatings qualitatively. The phase compositions were identified by using X-ray diffractometer XRD (D/max-rB, Japan) with a  $\text{Cu K}\alpha$  radiation (40 kV, 300 mA) with the scanning rate of  $3^\circ \text{ min}^{-1}$  and step size of  $0.01^\circ$ .

### 2.3. Microhardness and corrosion measurement

The microhardness was evaluated by using an HVS-1000 microhardness tester with Vickers inden-

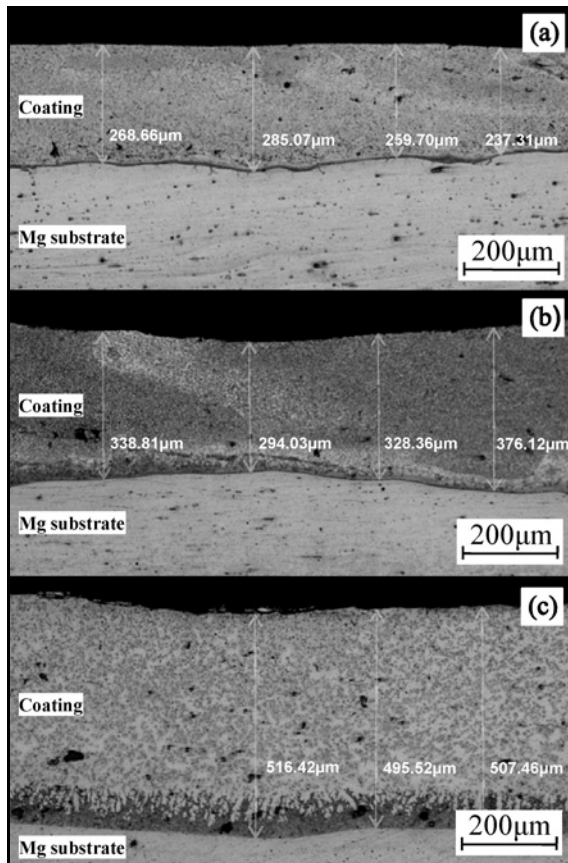


Fig. 2. The macrographs of the cladded coatings with different WC additions: (a) Al + 5 wt.% WC, (b) Al + 10 wt.% WC, and (c) Al + 15 wt.% WC.

ters, employing a constant load of 0.98 N for 15 s. The intervals of measured points were 60  $\mu\text{m}$  along the direction perpendicular to the laser coating surface. Every hardness value of the samples was determined with the average value of three measurement points.

Corrosion tests were performed on the AZ91D magnesium alloy and the laser cladding coatings by the CHI660E electrochemical workstation. A 1 mm deep groove was fabricated on the back of the corrosion specimen, which was twined around with copper wire as an electrode pole. Only 1 cm  $\times$  1 cm square experimental area on the coating surface was exposed, and the rest was wholly covered with one-component room temperature vulcanized silicone rubber. All the specimens were cleaned with alcohol before the corrosion test and then carried out in an aqueous 3.5 wt.% NaCl solution at room temperature (25  $^{\circ}\text{C}$ ). The corrosion cell with a three-electrode set-up consisted of a saturated calomel electrode as the reference electrode, a Pt sheet as the counter electrode and the specimen as the working electrode. The free corrosion potential was recorded for 10 min, and potential swept scope from  $-2.5$  to  $-0.5$  V at the scanning speed of 40  $\text{mV min}^{-1}$ .

### 3. Results and discussion

#### 3.1. Optical graphs of the cladded coatings

The optical images of the cross-section of the laser cladding coatings with 5, 10, and 15 wt.% WC additions are shown in Fig. 2. The coatings were cladded successfully on Mg substrates, and they were joined together by metallurgy bonding. The casting defects, including blowholes and cracks, were not found inside the coatings. Visible heat-affected zones were also not observed in the substrates close to the interfaces. The average thicknesses of the coatings were 263 and 334  $\mu\text{m}$  that were lower than the thickness of pre-coated powder (400  $\mu\text{m}$ ) at 5 and 10 wt.% WC additions (Figs. 2a,b). There was a higher increase at 15 wt.% WC addition, and the average thickness was 506  $\mu\text{m}$  (Fig. 2c), which is related to the increase of WC content with a high melting point. In the process of laser cladding, WC particles absorb more laser energy, and the energy absorbed by Al reduces relatively. The evaporation of Al is alleviated compared to the other two cladding processes, which make the coating thickness increase.

The magnified images of the different zones in the cladded coatings are shown in Fig. 3. In Fig. 3a, columnar crystals with like-lamellar structure grew perpendicular to the interface of substrate-coating, which was similar to directional solidification mode in casting. The number of particle phases in the upper coating was more than that in the lower coating. With the increase of WC content, in Fig. 3b, the black particle phases increased in quantity and became more extensive than those in Fig. 3a. At the content of 15 wt.% WC, lamellar eutectic microstructure and grey cellular microstructure were observed at the interface zone adjacent to the substrate (Fig. 3c). In the middle and top of the coating, tiny black and dark grey particle phases showed inhomogeneous size distribution with agglomeration tendency.

Only at 5 wt.% WC content (Fig. 3a) cracks were found in the substrate close to the interface. The reasons for cracks may be that the substrate was heated seriously when the coating was thin and had an expansion in the process of laser cladding followed by severe contraction due to rapid cooling, but the shrinkage was hindered by the coating, and ultimately stress concentration led to the appearance of cracks.

#### 3.2. X-ray diffraction analysis

The XRD patterns of the cladded coatings with WC additions of 5, 10, and 15 wt.% are shown in Fig. 4. Not only WC, which was used as the main ceramic reinforced phase in the predesigned scheme, was found, but also  $\text{Al}_{18}\text{Mg}_3\text{W}_2$  was also detected in all patterns. This means WC was decomposed in

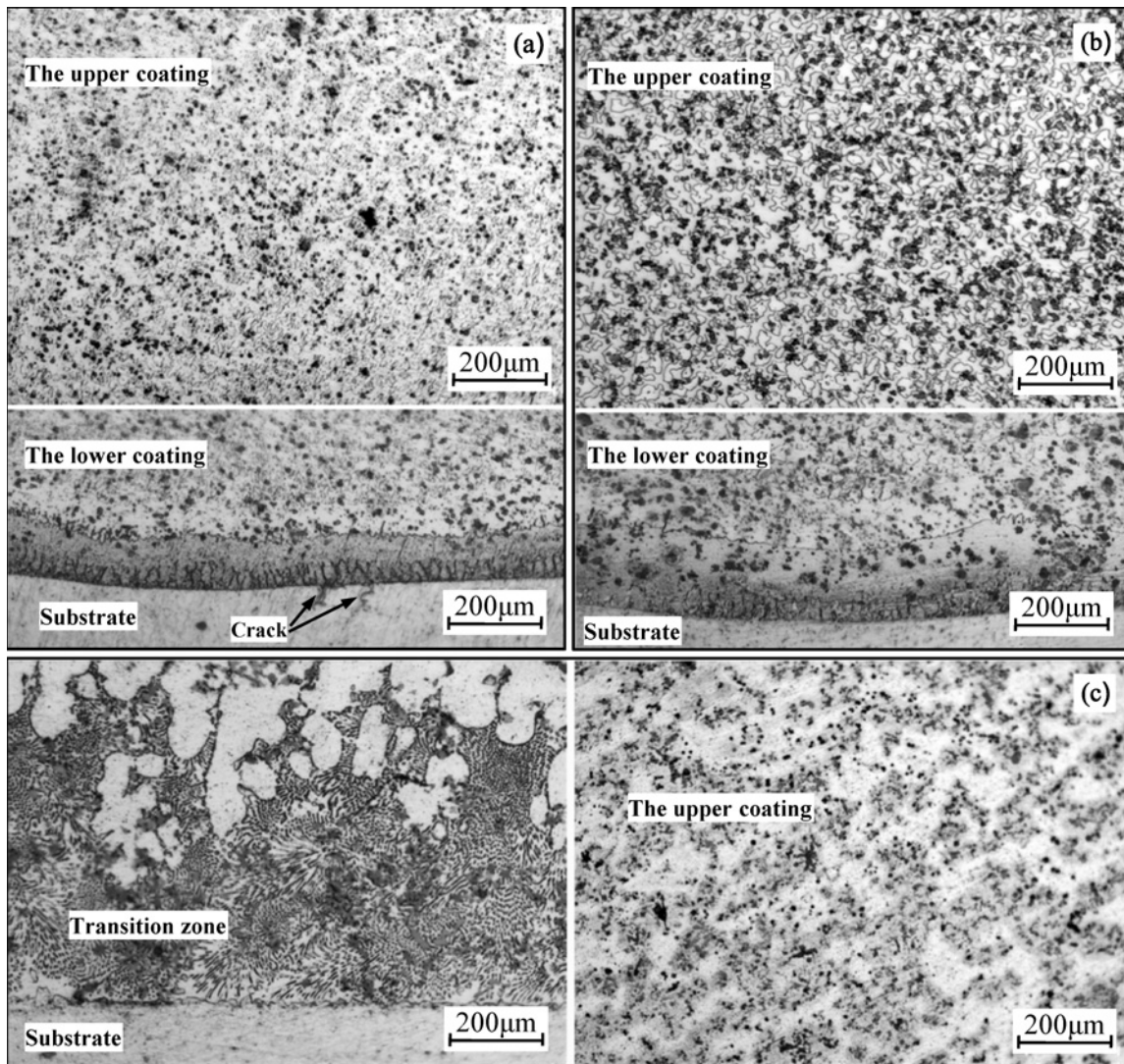


Fig. 3. The magnified images of the different zones in the cladded coatings: (a) Al + 5 wt.% WC, (b) Al + 10 wt.% WC, and (c) Al + 15 wt.% WC.

varying degrees during the laser cladding process, and dissociative tungsten reacted with Al and Mg to form intermetallic compound  $\text{Al}_{18}\text{Mg}_3\text{W}_2$ . The characteristic peaks corresponding to  $\alpha$ -Al,  $\alpha$ -Mg,  $\text{Al}_3\text{Mg}_2$ , and  $\text{Al}_{12}\text{Mg}_{17}$  were also identified in all patterns besides the mentioned above.  $\text{Al}_4\text{W}$  was observed at the content of Al + 10 wt.% WC (Fig. 4b). The intensity of diffraction peaks corresponding to  $\text{Al}_4\text{W}$  increased with the WC content added to 15 wt.% (Fig. 4c). This should be related to the reduction of the weight ratio of Al to WC in mixture powders.

### 3.3. SEM microstructures and EDS analysis

EDS measurement results of Al, Mg, and W contents (wt.%) at different positions of the coatings are shown in Fig. 5. The rectangular boxes marked with letters “B”, “M”, and “T” refer to the bottom, mid-

dle, and top areas detected by EDS and data results are displayed in the side of the boxes.

The laser cladding coating is composed of melted cladding powders and a part of the molten substrate. Mg element deriving from the substrate is redistributed inside the coating by stir, convection, and diffusion in the process of laser heating and cooling. The contents of Mg were different in different positions. At the position “B”, the contents were slightly higher than at the other positions “M” and “T” because this position was closer to the substrate. The highest value of Mg content was 30.94 wt.% at the position “B” at the coating with 15 wt.% WC, and the lowest value was 20.77 wt.% at the position “M” at the coating with 5 wt.% WC. The reverse trend was observed for Al concentration, which was between 59.09 wt.% (“B” at the coating with 15 wt.% WC) and 74.48 wt.% (“M” at the coating with 5 wt.% WC).

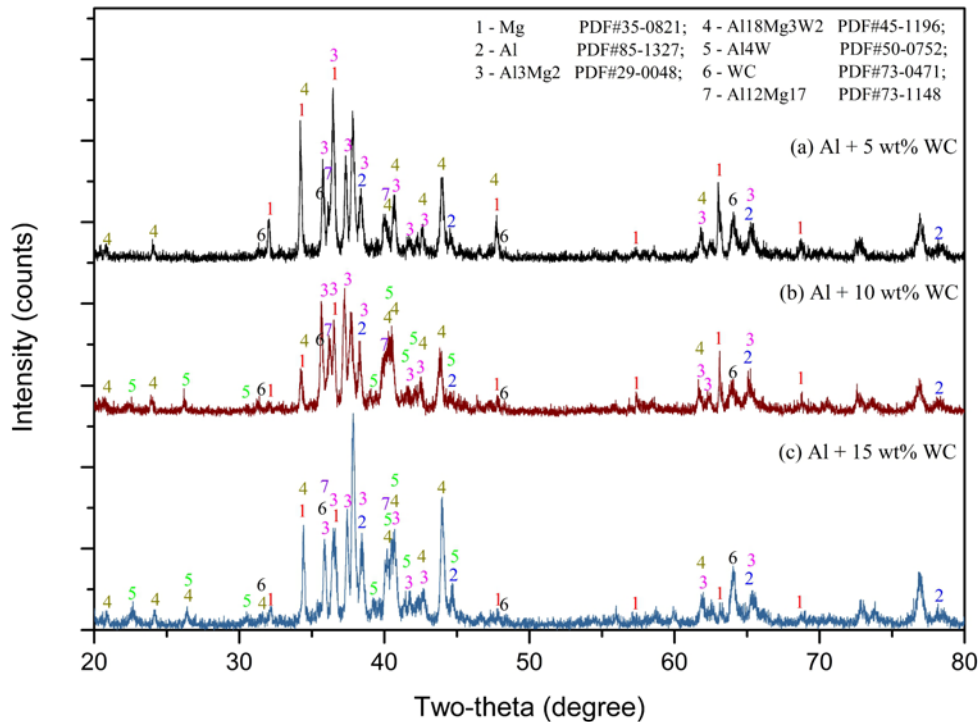


Fig. 4. The XRD patterns of the laser cladding coatings: (a) Al + 5 wt.% WC, (b) Al + 10 wt.% WC, and (c) Al + 15 wt.% WC.

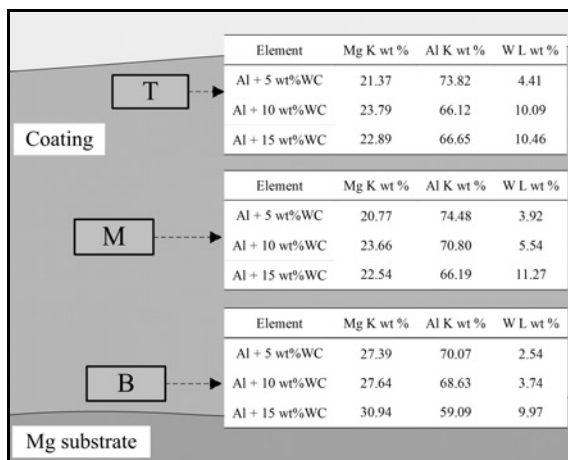


Fig. 5. EDS analysis at the bottom, middle, top positions of the cladded coatings.

Compared to the test results obtained by M. Hazra et al. [19] and Y. H. Liu et al. [26], in which Mg concentration in most positions of the cladded layers was in the range of 70–85 wt.% and Al concentration was lower than 20 wt.%, less Mg and more Al are detected in the coatings in the present results.

The increase of Mg content and the decrease of Al content could deteriorate the corrosion resistance of the coating. Less Mg and more Al in this research may attribute to the evaporation of Mg element during laser processing and the control of volume fraction

of the melted substrate metal by appropriate parameters setting and the application of low power pulse YAG laser. The contents of W were the lowest at the position “B” in three coatings and increased gradually from the bottom to top areas except for the coating with Al + 15 wt.% WC, in which W contents were relatively high at all three positions.

### 3.3.1. Microstructures at the bottom of the coatings

Figure 6 shows magnified SEM micrographs at the bottom areas of the coatings. Elements concentrations of the microstructures analyzed by EDS are shown in Table 3. Typical eutectic microstructure was observed in the bottom of the coatings with 15 wt.% WC addition adjacent to Mg substrate (Figs. 6b,c), which can be proved by EDS analysis for spot 4: Mg-62.87, Al-36.92 and W-0.16 (at.%) and the binary Al-Mg alloy phase diagram (Fig. 7). In the bottom, the compositions of Mg and Al fall near Al-Mg eutectic point composition from the phase diagram, and a eutectic reaction occurs. The eutectic microstructure was composed of Al<sub>12</sub>Mg<sub>17</sub> and Mg solid solution. Dark gray rodlike structures were found in Fig 6a. EDS analysis for spot 1 showed the content of Mg-70.56, Al-29.19, and W-0.25 (at.%), which were considered as a solid solution of Al in Mg. So, microstructure in the bottom of the coating with 5 wt.% WC addition was also identified as an atypical eutectic structure. Massive

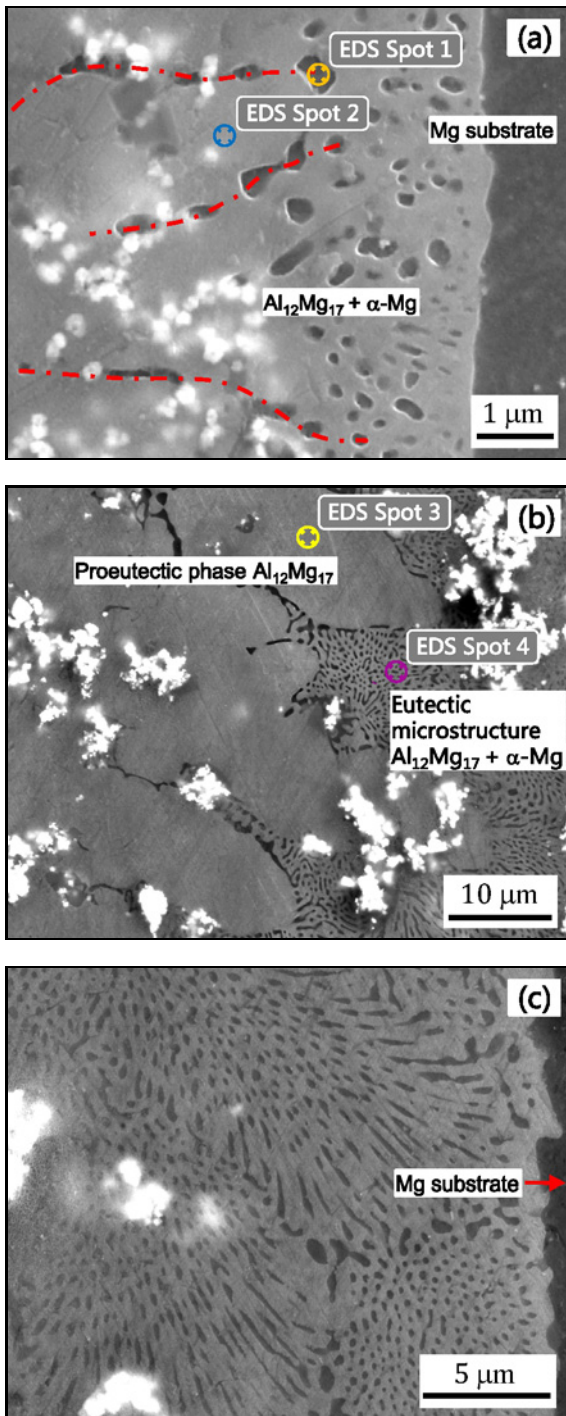


Fig. 6. SEM micrographs and EDS positions at the bottom areas of the coatings: (a) Al + 5 wt.% WC, (b) Al + 15 wt.% WC, and (c) magnified eutectic microstructure at Al + 15 wt.% WC.

light gray phases were also found at the position close to the eutectic microstructure in Figs. 6a,b. According to EDS detection results of spot 2 and spot 3 and Al-Mg phase diagram, massive light gray phases were regarded as proeutectic phase  $\text{Al}_{12}\text{Mg}_{17}$ , which was

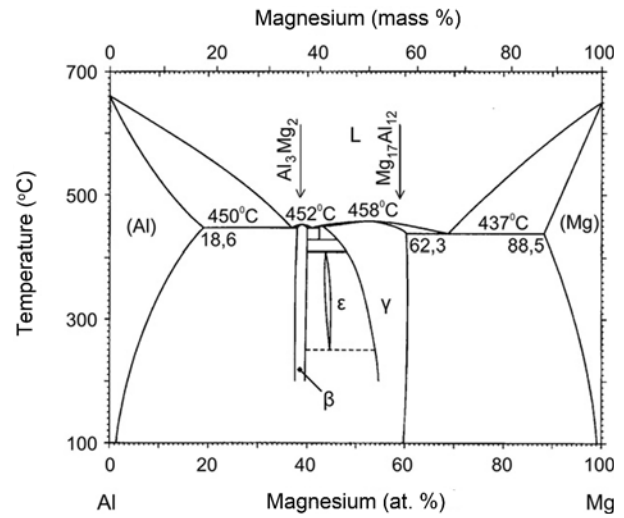


Fig. 7. Phase diagram of the Al-Mg system [27].

crystallized preferentially from molten coatings metal. A small amount of rodlike Mg solid solution which corresponded to like-lamellar microstructure identified in Fig. 3a was precipitated from  $\text{Al}_{12}\text{Mg}_{17}$  in a later stage of crystallization. The morphology of the proeutectic phase in this study is also similar to that in the cladded coating using Al-Si powders [10].

### 3.3.2. Microstructures at the upper part of the coatings

Microstructures at the upper part of the coatings with different WC addition are shown in Fig. 8. Elements concentrations of Mg, Al, and W are exhibited in Table 4.

At 5 wt.% WC addition (Fig. 8a), a large number of tiny white particles distributed uniformly on the gray matrix, whose size was between 400 and 500 nm. EDS analysis for spot 1 showed the contents of Al-69.88, Mg-28.68, and W-1.44 (at.%). According to XRD results, the tiny particles were considered as intermetallic compound  $\text{Al}_{18}\text{Mg}_3\text{W}_2$ . The atomic contents of Al and Mg by EDS measurement were higher than the ideal stoichiometry ratio of  $\text{Al}_{18}\text{Mg}_3\text{W}_2$ , which may be because the EDS detection radius is more significant than particle radius and Al and Mg in the surrounding matrix are detected.

At 10 wt.% WC addition (Fig. 8b), the quantities of tiny particles decreased, and brighter white particles were found. These particles showed a high tendency to agglomerate into large particles. EDS analysis for spot 2 indicated that a brighter white particle contained 33.35 at.% Mg, 54.84 at.% Al, and more W-11.8 at.%. The composition and XRD analysis indicated the formation of an intermetallic compound  $\text{Al}_4\text{W}$ . The gray matrix was not uniform: part of the matrix was dark gray, as shown in the position of spot

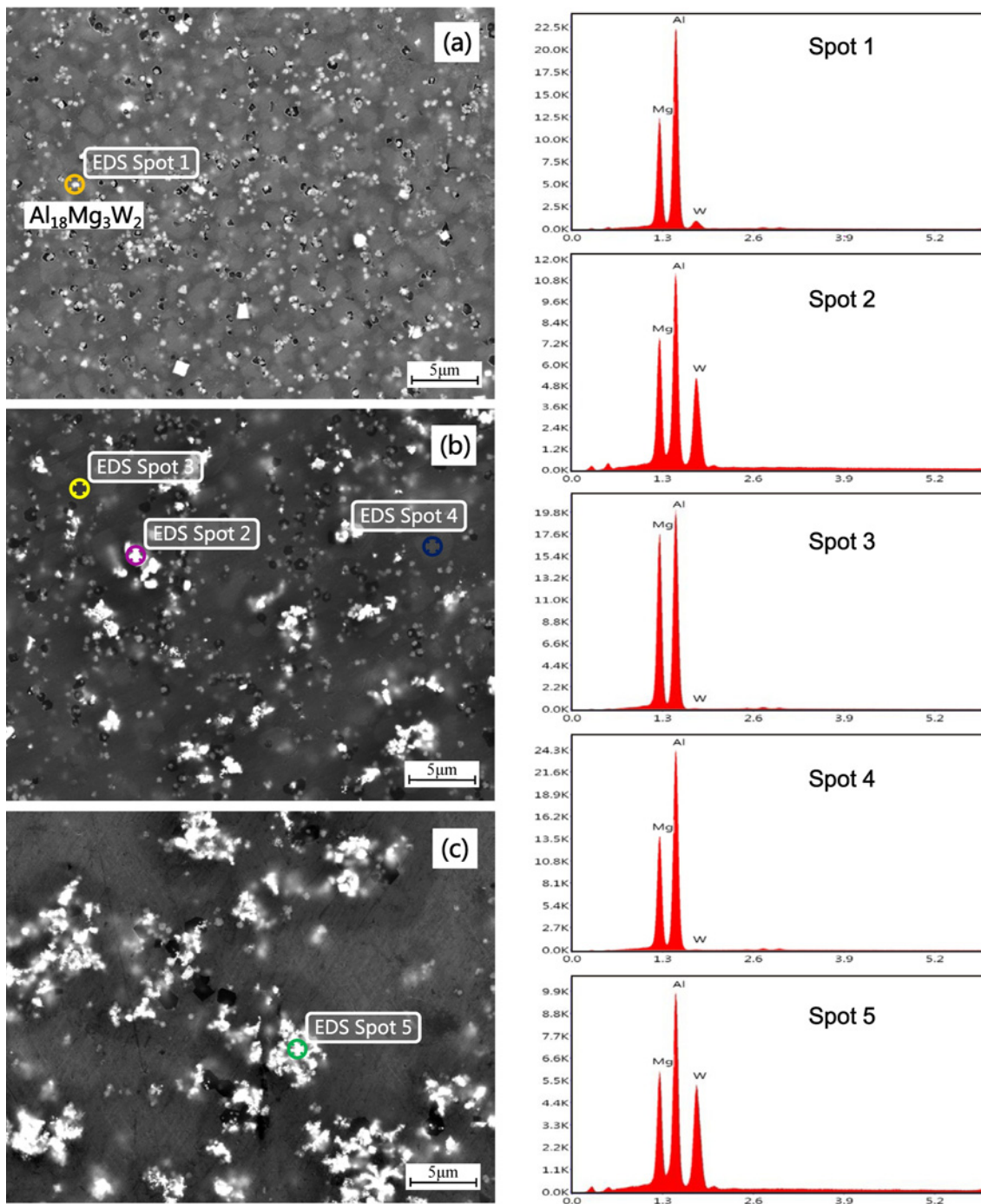


Fig. 8. Typical SEM micrographs and EDS spectra of the laser cladding coating layers for different samples: (a) Al + 5 wt.% WC, (b) Al + 10 wt.% WC, and (c) Al + 15 wt.% WC.

Table 3. Elements concentrations of the microstructures analyzed by EDS

Locations	Mg K		Al K		W L	
	(wt.%)	(at.%)	(wt.%)	(at.%)	(wt.%)	(at.%)
Spot 1	67.29	70.56	30.90	29.19	1.81	0.25
Spot 2	65.17	68.43	33.12	31.34	1.71	0.24
Spot 3	59.80	62.82	39.12	37.03	1.08	0.15
Spot 4	59.68	62.87	38.91	36.92	1.17	0.16

Table 4. Elements concentration of the microstructure analyzed by EDS (at.%)

Locations	Mg K	Al K	W L
Spot 1	28.68	69.88	1.44
Spot 2	33.35	54.84	11.80
Spot 3	35.93	63.96	0.12
Spot 4	28.60	71.28	0.12
Spot 5	31.14	55.67	13.18

3; part of the matrix was light gray, as shown in the position of spot 4. EDS revealed the composition of spot 3: Mg-35.93, Al-63.96, and W-0.12 (at.%) and the composition of spot 4: Mg-28.60, Al-71.28 and W-0.12 (at.%). According to the binary phase diagram (Fig. 7), the matrix was identified as a mixture of  $Al_3Mg_2$  and a solid solution of Mg in Al. More Mg was contained in the dark gray zone, and more Al existed in the light gray zone. A similar matrix appearance was also observed in Fig. 8a.

At 15 wt.% WC addition (Fig. 8c), brighter white particles agglomerated into larger size particles and the number increased significantly than at 10 wt.% WC addition, which was also identified as  $Al_4W$  based on the element's contents of spot 5 of Mg-31.14, Al-55.67, and W-13.18 (at.%). Tiny white particles  $Al_{18}Mg_3W_2$  were almost not observed. Though WC particle was expected as the ceramic reinforcement phase to improve coating performance, the test results approved, which was decomposed almost entirely during laser cladding. Independently existing WC particle was not found in the coatings and was replaced by  $Al_{18}Mg_3W_2$  and/or  $Al_4W$ .

### 3.4. Micro-hardness analysis

Figure 9 shows the micro-hardness along the cross-section of the coatings with different WC addition. After laser cladding, the hardness of the coatings improved significantly compared with that of the Mg substrate. The hardness values varied from 205 to 260 HV in the coatings with 5 and 10 wt.% WC. Near the interface, the hardness increased. The reason may be that the density of WC is far higher than that of Al, which inclines to sink to the bottom of the melting pool. The increase of W content near the interface results in the increase of the hardness. No transition zones were observed from the coatings to the substrate, and the hardness dropped sharply. At 15 wt.% WC addition, the thickness of the coating increased because more Mg substrate was melted into the coating, and the decrease of the hardness along the cross-section of the coating became gentle. The maximum value (262 HV) was found near the surface of the coat-

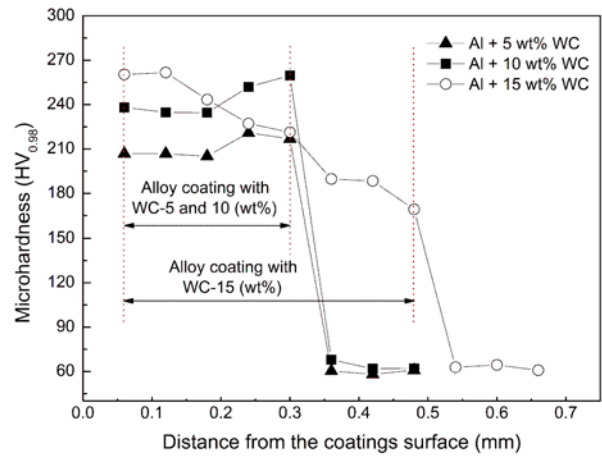
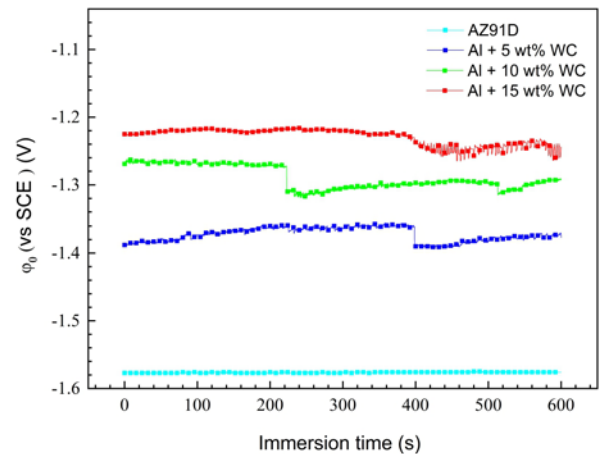


Fig. 9. Micro-hardness along the cross-section of the laser cladding coatings.

Fig. 10. The open circuit potentials ( $\varphi_0$ ) of the substrate and the coatings with different WC contents in 3.5% NaCl solution.

ing, which was about 4 times that of the substrate (63 HV).

### 3.5. Corrosion behavior

#### 3.5.1. Open circuit potential

The relation of corrosion potential to time in 3.5% NaCl solution at zero current density for the laser cladding coatings and Mg substrate is shown in Fig. 10. The open-circuit potential ( $\varphi_0$ ) of AZ91D Mg alloy was almost stabilized at  $-1.576$  V, and  $\varphi_0$  values of the coatings varied from  $-1.388$  to  $-1.216$  V at 0 to 600 s. The shift of  $\varphi_0$  to positive potential may increase the corrosion resistance of the coatings.

#### 3.5.2. Polarization curve

Potentiodynamic polarization curves of the sub-

Table 5. Corresponding electrochemical constants

Sample	$E_{\text{corr}}$ (V)	$i_{\text{corr}}$ ( $\text{A cm}^{-2}$ )	$i_{\text{p}}$ ( $\text{A cm}^{-2}$ )	$E_{\text{pit}}$ (V)	$E_{\text{pit}} - E_{\text{corr}}$ (mV)
Al + 5 wt.% WC	-1.184	$3.308 \times 10^{-5}$	$2.882 \times 10^{-5}$	-0.9954	0.1886
Al + 10 wt. % WC	-1.191	$3.020 \times 10^{-5}$	$2.373 \times 10^{-5}$	-0.9172	0.2738
Al + 15 wt.% WC	-1.168	$1.476 \times 10^{-5}$	$1.511 \times 10^{-5}$	-0.9582	0.2098
AZ91D	-1.499	$1.444 \times 10^{-4}$	–	–	–

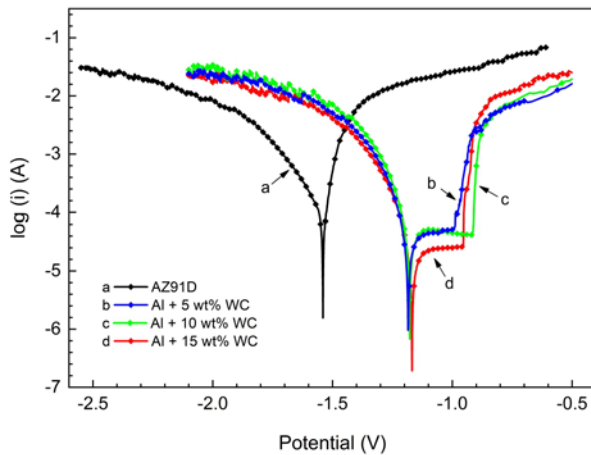


Fig. 11. Potentiodynamic polarization curves of AZ91D Mg alloy substrate and the laser cladding coatings with 5, 10, and 15 wt.% WC additions in 3.5% NaCl solution.

strate and the coatings measured by the method of linear sweep voltammetry in 3.5 % NaCl solution are shown in Fig. 11. The electrochemical parameters of the coatings and the substrate are shown in Table 5. The polarization curve of the Mg substrate was located at the top-left of that of the coatings, as shown in Fig. 11. Free corrosion potential  $E_{\text{corr}}$  was the lowest, and corrosion current density  $i_{\text{corr}}$  was the highest, as shown in Table 5, which indicated that AZ91D Mg alloy could be corroded easily and rapidly. The loose and porous oxidation product of Mg alloy cannot well prevent unoxidized Mg from corroding when exposed to corrosive medium [28, 29].

After laser cladding, corrosion resistance of the coatings was improved significantly. Free corrosion potential  $E_{\text{corr}}$  raised by 0.308–0.331 V and corrosion current density  $i_{\text{corr}}$  increased by one order of magnitude compared to the Mg substrate, and the passivation phenomenon of the coatings was also observed from Figs. 11b, c, and d. Maintaining passivity current density  $i_{\text{p}}$  of the coatings was very close to each other, and only at 15 wt.% WC addition  $i_{\text{p}}$  decreased slightly. The lower the value of  $i_{\text{p}}$ , the slower the corrosion rate of passivation material is. Therefore, from this point, corrosion resistance of the coating with 15 wt.% WC was more excellent than the others. With the increase of potential, pitting corrosion occurred in the coatings when the passivation film was penetrated due to the

function of erosive anion  $\text{Cl}^-$ . Pitting corrosion potential  $E_{\text{pit}}$  is defined as the potential at the inflection point of the polarization curve from horizontal to vertical. The maximum of  $E_{\text{pit}}$  was  $-0.9172$  V, which was found at the coating with 10 wt.% WC and the maximal potential difference between  $E_{\text{pit}}$  and  $E_{\text{corr}}$  was also found in this coating. Consequently, from the capability of pitting resistance, the coating with 10 wt.% WC addition was superior to the others, and the passivation film was hard to be penetrated.

#### 4. Conclusions

Laser surface cladding of AZ91D magnesium alloy was carried out with Al-WC mixture powders by a low power pulsed Nd: YAG laser. The microstructure, phases composition, micro-hardness, and corrosion resistance of the coatings were investigated. The following conclusions can be drawn:

1. Most of the WC was decomposed during the process of laser cladding. New tungsten-containing intermetallic compounds  $\text{Al}_{18}\text{Mg}_3\text{W}_2$  and  $\text{Al}_4\text{W}$  were formed in the coatings.  $\text{Al}_{18}\text{Mg}_3\text{W}_2$  was substituted by  $\text{Al}_4\text{W}$  gradually with the increase of WC weight fraction.  $\alpha\text{-Al}$ ,  $\alpha\text{-Mg}$ ,  $\text{Al}_3\text{Mg}_2$ , and  $\text{Al}_{12}\text{Mg}_{17}$  were also found at the coatings besides mentioned above.
2. The size of tiny white particles  $\text{Al}_{18}\text{Mg}_3\text{W}_2$  was between 400 and 500 nm. Bright white particles  $\text{Al}_4\text{W}$  agglomerate into large particles, and the tendency of clustering increased with the increase of WC content.
3. The micro-hardness of the alloy coating increased compared with that of the AZ91D magnesium alloy substrate. The corrosion resistance of the coatings was also improved significantly, and the passivation phenomenon was observed in all coatings.

#### Acknowledgement

This work was financially supported by the Natural Science Foundation of Shanxi Province of China (201901D111174).

#### References

- [1] H. Pan, Y. Ren, H. Fu, H. Zhao, L. Wang, X. Meng, G. Qin, Recent developments in rare-earth

- free wrought magnesium alloys having high strength: A review, *J. Alloy Compd.* 663 (2016) 321–331. [doi:10.1016/j.jallcom.2015.12.057](https://doi.org/10.1016/j.jallcom.2015.12.057)
- [2] F. Czerwinski, Controlling the ignition and flammability of magnesium for aerospace applications, *Corros. Sci.* 86 (2014) 1–16. [doi:10.1016/j.corsci.2014.04.047](https://doi.org/10.1016/j.corsci.2014.04.047)
- [3] T. F. Kubatík, F. Lukáč, J. Stoužil, P. Ctibor, F. Průša, K. Stehlíková, Preparation and properties of plasma sprayed NiAl10 and NiAl40 coatings on AZ91 substrate, *Surf. Coat. Tech.* 319 (2017) 145–154. [doi:10.1016/j.surfcoat.2017.03.064](https://doi.org/10.1016/j.surfcoat.2017.03.064)
- [4] Y. Zhou, J. Xiong, F. Yan, The preparation and characterization of a nano-CeO<sub>2</sub>/phosphate composite coating on magnesium alloy AZ91D, *Surf. Coat. Tech.* 328 (2017) 335–343. [doi:10.1016/j.surfcoat.2017.09.014](https://doi.org/10.1016/j.surfcoat.2017.09.014)
- [5] A. Da Forno, M. Bestetti, Effect of the electrolytic solution composition on the performance of micro-arc anodic oxidation films formed on AM60B magnesium alloy, *Surf. Coat. Tech.* 205 (2010) 1783–1788. [doi:10.1016/j.surfcoat.2010.05.043](https://doi.org/10.1016/j.surfcoat.2010.05.043)
- [6] Y. L. Kuo, K. H. Chang, Atmospheric pressure plasma enhanced chemical vapor deposition of SiO<sub>x</sub> films for improved corrosion resistant properties of AZ31 magnesium alloys, *Surf. Coat. Tech.* 283 (2015) 194–200. [doi:10.1016/j.surfcoat.2015.11.004](https://doi.org/10.1016/j.surfcoat.2015.11.004)
- [7] Y. Gao, C. Wang, H. Pang, H. Liu, M. Yao, Broad-beam laser cladding of Al-Cu alloy coating on AZ91HP magnesium alloy, *Appl. Surf. Sci.* 253 (2007) 4917–4922. [doi:10.1016/j.apsusc.2006.10.075](https://doi.org/10.1016/j.apsusc.2006.10.075)
- [8] G. Rolink, A. Weisheit, T. Biermann, K. Bobzin, M. Öte, T. F. Linke, C. Schulz, I. Kelbassa, Investigations of laser clad, thermal sprayed and laser remelted AlSi20-coatings on magnesium alloy AZ31B under constant and cycling thermal load, *Surf. Coat. Tech.* 259 Part C (2014) 751–758. [doi:10.1016/j.surfcoat.2014.09.049](https://doi.org/10.1016/j.surfcoat.2014.09.049)
- [9] E. Chen, K. Zhang, J. Zou, Laser cladding of a Mg based Mg-Gd-Y-Zr alloy with Al-Si powders, *Appl. Surf. Sci.* 367 (2016) 11–18. [doi:10.1016/j.apsusc.2016.01.124](https://doi.org/10.1016/j.apsusc.2016.01.124)
- [10] A. Dziadoń, R. Mola, L. Błaż, The microstructure of the surface layer of magnesium laser alloyed with aluminum and silicon, *Mater. Charact.* 118 (2016) 505–513. [doi:10.1016/j.matchar.2016.06.034](https://doi.org/10.1016/j.matchar.2016.06.034)
- [11] L. Q. Wang, J. S. Zhou, J. Liang, J. M. Chen, Characterization and electrochemical corrosion properties of Sn and Al + Sn containing coatings on magnesium alloys prepared by laser surface treatment, *Mater. Corros.* 65 (2014) 820–827. [doi:10.1002/maco.201307092](https://doi.org/10.1002/maco.201307092)
- [12] T. M. Yue, T. Li, Laser cladding of Ni/Cu/Al functionally graded coating on magnesium substrate, *Surf. Coat. Tech.* 202 (2008) 3043–3049. [doi:10.1016/j.surfcoat.2007.11.007](https://doi.org/10.1016/j.surfcoat.2007.11.007)
- [13] C. Wang, Y. Chen, T. Li, B. Yao, Composition design and laser cladding of Ni-Zr-Al alloy coating on the magnesium surface, *Appl. Surf. Sci.* 256 (2009) 1609–1613. [doi:10.1016/j.apsusc.2009.09.029](https://doi.org/10.1016/j.apsusc.2009.09.029)
- [14] C. Wang, T. Li, B. Yao, R. Wang, C. Dong, Laser cladding of eutectic-based Ti-Ni-Al alloy coating on magnesium surface, *Surf. Coat. Tech.* 205 (2010) 189–194. [doi:10.1016/j.surfcoat.2010.06.032](https://doi.org/10.1016/j.surfcoat.2010.06.032)
- [15] J. D. Majumdar, B. R. Chandra, R. Galun, B. L. Mordike, I. Manna, Laser composite surfacing of a magnesium alloy with silicon carbide, *Compos. Sci. Technol.* 63 (2003) 771–778. [doi:10.1016/S0266-3538\(02\)00266-X](https://doi.org/10.1016/S0266-3538(02)00266-X)
- [16] Y. L. Gao, C. S. Wang, M. Yao, H. B. Liu, The resistance to wear and corrosion of laser-cladding Al<sub>2</sub>O<sub>3</sub> ceramic coating on Mg alloy, *Appl. Surf. Sci.* 253 (2007) 5306–5311. [doi:10.1016/j.apsusc.2006.12.001](https://doi.org/10.1016/j.apsusc.2006.12.001)
- [17] Y. Guo, Y. Zhang, Z. Li, S. Wei, T. Zhang, L. Yang, S. Liu, Microstructure and properties of in-situ synthesized ZrC-Al<sub>3</sub>Zr reinforced composite coating on AZ91D magnesium alloy by laser cladding, *Surf. Coat. Tech.* 334 (2018) 471–478. [doi:10.1016/j.surfcoat.2017.12.007](https://doi.org/10.1016/j.surfcoat.2017.12.007)
- [18] L. Yang, Z. Li, Y. Zhang, S. Wei, F. Liu, Al-TiC in situ composite coating fabricated by low power pulsed laser cladding on AZ91D magnesium alloy, *Appl. Surf. Sci.* 435 (2018) 1187–1198. [doi:10.1016/j.apsusc.2017.11.240](https://doi.org/10.1016/j.apsusc.2017.11.240)
- [19] M. Hazra, A. K. Mondal, S. Kumar, C. Blawert, N. B. Dahotre, Laser surface cladding of MRI 153M magnesium alloy with (Al+Al<sub>2</sub>O<sub>3</sub>), *Surf. Coat. Tech.* 203 (2009) 2292–2299. [doi:10.1016/j.surfcoat.2009.02.022](https://doi.org/10.1016/j.surfcoat.2009.02.022)
- [20] B. J. Zheng, X. M. Chen, J. S. Lian, Microstructure and wear property of laser cladding Al + SiC powders on AZ91D magnesium alloy, *Opt. Laser Eng.* 48 (2010) 526–532. [doi:10.1016/j.optlaseng.2010.01.001](https://doi.org/10.1016/j.optlaseng.2010.01.001)
- [21] A. Riquelme, P. Rodrigo, M. D. Escalera-Rodríguez, J. Rams, Analysis and optimization of process parameters in Al-SiCp laser cladding, *Opt. Laser Eng.* 78 (2016) 165–173. [doi:10.1016/j.optlaseng.2015.10.014](https://doi.org/10.1016/j.optlaseng.2015.10.014)
- [22] J. Qian, J. Zhang, S. Li, C. Wang, Study on laser cladding NiAl/Al<sub>2</sub>O<sub>3</sub> coating on magnesium alloy, *Rare Metal Mat. Eng.* 42 (2013) 466–469. [doi:10.1016/S1875-5372\(13\)60049-1](https://doi.org/10.1016/S1875-5372(13)60049-1)
- [23] J. Przybyłowicz, J. Kusiński, Structure of laser clad tungsten carbide composite coatings, *J. Mater. Process. Tech.* 109 (2001) 154–160. [doi:10.1016/S0924-0136\(00\)00790-1](https://doi.org/10.1016/S0924-0136(00)00790-1)
- [24] M. R. Fernández, A. García, J. M. Cuetos, R. González, A. Noriega, M. Cadenas, Effect of actual WC content on the reciprocating wear of a laser cladding NiCrBSi alloy reinforced with WC, *Wear* 324 (2015) 80–89. [doi:10.1016/j.wear.2014.12.021](https://doi.org/10.1016/j.wear.2014.12.021)
- [25] S. Hong, Y. Wu, B. Wang, Y. Zheng, W. Gao, G. Li, High-velocity oxygen-fuel spray parameter optimization of nanostructured WC-10Co-4Cr coatings and sliding wear behavior of the optimized coating, *Mater. Design* 55 (2014) 286–291. [doi:10.1016/j.matdes.2013.10.002](https://doi.org/10.1016/j.matdes.2013.10.002)
- [26] Y. H. Liu, Z. X. Guo, Y. Yang, H. Y. Wang, J. D. Hu, Y. X. Li, A. N. Chumakov, N. A. Bosak, Laser (a pulsed Nd:YAG) cladding of AZ91D magnesium alloy with Al and Al<sub>2</sub>O<sub>3</sub> powders, *Appl. Surf. Sci.* 253 (2006) 1722–1728. [doi:10.1016/j.apsusc.2006.03.003](https://doi.org/10.1016/j.apsusc.2006.03.003)
- [27] H. Okamoto, Al-Mg (aluminum-magnesium), *J. Phase Equilib. Diff.* 19 (1998) 598. [doi:10.1361/105497198770341815](https://doi.org/10.1361/105497198770341815)
- [28] M. Curioni, The behaviour of magnesium during free corrosion and potentiodynamic polarization investigated by real-time hydrogen measurement and optical imaging, *Electrochim. Acta* 120 (2014) 284–292. [doi:10.1016/j.electacta.2013.12.109](https://doi.org/10.1016/j.electacta.2013.12.109)

- [29] J. Li, B. Zhang, Q. Wei, N. Wang, B. Hou, Electrochemical behavior of Mg-Al-Zn-In alloy as anode materials in 3.5 wt.% NaCl solution, *Electrochim. Acta* 238 (2017) 156–167.  
[doi:10.1016/j.electacta.2017.03.119](https://doi.org/10.1016/j.electacta.2017.03.119)